Neuron
Report

Activity-Dependent Plasticity of the NMDA-Receptor Fractional Ca^{2+} Current

Aleksander Sobczyk[1,2] and Karel Svoboda[1,2,*]
[1] Howard Hughes Medical Institute, Cold Spring Harbor Laboratory, Cold Spring Harbor, NY 11724, USA
[2] Present address: Janelia Farm Research Campus, Howard Hughes Medical Institute, 19700 Helix Drive, Ashburn, VA 20147, USA.
*Correspondence: svobodak@janelia.hhmi.org
DOI 10.1016/j.neuron.2006.11.016

SUMMARY

Ca^{2+} influx through NMDA receptors (NMDA-Rs) triggers synaptic plasticity, gene transcription, and cytotoxicity, but little is known about the regulation of NMDA-Rs themselves. We used two-photon glutamate uncaging to activate NMDA-Rs on individual dendritic spines in rat CA1 neurons while we measured NMDA-R currents at the soma and [Ca^{2+}] changes in spines. Low-frequency uncaging trains induced Ca^{2+}-dependent long-term depression of NMDA-R-mediated synaptic currents. Additionally, uncaging trains caused a reduction in the Ca^{2+} accumulation per unit of NMDA-R current in spines due to a reduction in the fraction of the NMDA-R current carried by Ca^{2+}. Induction of depression of NMDA-R-mediated Ca^{2+} influx required activation of NR2B-containing receptors. Receptors in single spines depressed rapidly in an all-or-none manner. These adaptive changes in NMDA-R function likely play a critical role in metaplasticity and in stabilizing activity levels in neuronal networks with Hebbian synapses.

INTRODUCTION

Correlated presynaptic and postsynaptic activity can induce the long-term potentiation (LTP) and depression (LTD) of AMPA-R-mediated synaptic transmission (Malenka and Bear, 2004). LTP and LTD may underlie aspects of memory and other forms of cognitive plasticity (Bliss and Collingridge, 1993). Activation of *N*-methyl-*D*-aspartate receptors (NMDA-Rs) is critical for the induction of LTP (Collingridge et al., 1983; Cummings et al., 1996) and LTD (Dudek and Bear, 1992) as well as gene transcription (Ghosh et al., 1994), cytotoxicity (Vanhoutte and Bading, 2003), and morphogenesis (Engert and Bonhoeffer, 1999; Maletic-Savatic et al., 1999; Yuste and Bonhoeffer, 2001). A substantial fraction of the current through NMDA-Rs is carried by Ca^{2+} ions (fractional Ca^{2+} current, ~10%) (Garaschuk et al., 1996; Schneggenburger et al., 1993). As a result, NMDA-R activation can lead to large Ca^{2+} accumulations in dendritic spines (Muller and Connor, 1991; Noguchi et al., 2005; Sabatini et al., 2002; Sobczyk et al., 2005; Yuste and Denk, 1995), triggering the induction of LTP and LTD (Malenka and Bear, 2004; Zucker, 1999). NMDA-Rs also carry a substantial fraction of the total synaptic charge (Hestrin et al., 1990) and may be critical for recurrent excitation in cortical networks (Wang, 2002). Despite their importance, relatively little is known about the regulation of NMDA-Rs themselves.

At cortical synapses, NMDA-Rs are heterotetramers comprised of two copies of the obligatory NR1 subunit and a combination of NR2A or NR2B subunits (Cull-Candy et al., 2001; Kutsuwada et al., 1992). Over development, NR2B-rich receptors are supplemented with NR2A subunits (Monyer et al., 1994; Quinlan et al., 1999; Sheng et al., 1994). Populations of NMDA-Rs in individual CA1 spines can have different fractional Ca^{2+} currents, and this is explained in part by the heterogeneity in subunit composition across spines (Sobczyk et al., 2005).

NMDA-Rs appear to be relatively stable at synapses (Kullmann, 2003). Synaptic stimuli that induce LTP, measured as an increase in AMPA-R-mediated excitatory postsynaptic currents (EPSCs), typically leave NMDA-Rs unchanged (Kauer et al., 1988). NMDA-R-mediated EPSCs express activity-dependent long-term depression (LTD_{NMDA-R}), but the changes in NMDA-R EPSCs are modest (~30%) (Montgomery et al., 2005; Morishita et al., 2005; Selig et al., 1995). Consistently, the number of AMPA-Rs per synapse varies dramatically between individual synapses (Matsuzaki et al., 2001; Nusser et al., 1998; Takumi et al., 1999), whereas the number of NMDA-Rs is much less variable (Nimchinsky et al., 2004; Noguchi et al., 2005; Racca et al., 2000; Sobczyk et al., 2005).

Because NMDA-R-mediated Ca^{2+} accumulations in dendritic spines are of particular functional significance, we performed experiments to determine whether they can be independently modulated in a use-dependent manner. Low-frequency activation of NMDA-Rs induced LTD_{NMDA-R}, and in addition depressed the fraction of the NMDA-R current carried by Ca^{2+}. Moreover, populations of NMDA-Rs in individual spines depressed in an all-or-none manner.

RESULTS

To probe NMDA-Rs we combined (Carter and Sabatini, 2004; Noguchi et al., 2005; Sobczyk et al., 2005) two-photon glutamate uncaging with whole-cell measurements of synaptic currents (Furuta et al., 1999; Matsuzaki et al., 2001) and two-photon [Ca^{2+}] imaging (Mainen et al., 1999b; Yasuda et al., 2004; Yuste and Denk, 1995). This allowed us to stimulate NMDA-Rs on single spines while we measured the amplitudes of uncaging-evoked currents at the soma (ΔuEPSC) and the amplitudes of Ca^{2+} accumulations in individual spines (Δ[Ca^{2+}]).

CA1 pyramidal cells in hippocampal brain slices (postnatal day 16–17) were loaded with low-affinity Ca^{2+}-sensitive (green fluorescence, *G*; 500 μM Fluo4FF) and Ca^{2+}-insensitive (red fluorescence, *R*; 30 μM Alexa 594) fluorophores through the whole-cell recording pipette (Figure 1A). Spines on secondary or tertiary apical dendrites were visualized in the red fluorescence channel (Figure 1A, inset). To ensure favorable conditions for voltage-clamp recordings and consistent and stable concentrations of the Ca^{2+} indicator, we imaged spines that were relatively close to the patch pipette (within 150 μm), starting at least 20 min after break-in. [Ca^{2+}] imaging in spines and their parent dendrites was performed in line scan mode (see Experimental Procedures). Red fluorescence was constant during the entire acquisition period (Figure 1B). [Ca^{2+}] was quantified as the change in green fluorescence expressed as the percentage of the maximum fluorescence at saturating Ca^{2+} (see Experimental Procedures). Under our experimental conditions, even the largest [Ca^{2+}] transients were in the linear range of the indicator (<20%), implying that fluorescence changes were proportional to [Ca^{2+}] (Yasuda et al., 2004).

To selectively stimulate glutamate receptors on individual targeted spines, we uncaged MNI-glutamate next to spine heads that were well separated from their parent dendrite and other spines (Sobczyk et al., 2005) (see Experimental Procedures). These stimuli faithfully mimic the time course of glutamate-receptor activation during synaptic stimulation (Carter and Sabatini, 2004; Matsuzaki et al., 2001; Sobczyk et al., 2005). Experiments were performed in voltage clamp in the presence of AMPA-R blockers, drugs to reduce membrane excitation, nonlinearities, low Mg^{2+}, and inhibitors of Ca^{2+} release from intracellular stores (see Experimental Procedures and [Sobczyk et al., 2005]). Uncaging-evoked postsynaptic currents were kept small (amplitude: ΔuEPSC <8 pA; median: 4.4 ± 0.5 pA), minimizing the possibility of uncaging-evoked membrane depolarization in spines and activation of voltage-gated Ca^{2+} channels (VGCCs). Extensive control experiments have shown that under these conditions, uEPSCs and [Ca^{2+}] transients were produced entirely by NMDA-Rs (Figure S1 in the Supplemental Data available with this article online) (also Figures S1 and S6 in [Sobczyk et al., 2005]). Uncaging at low frequencies (0.05 Hz) reliably induced uEPSCs and [Ca^{2+}] transients that were mostly restricted to the stimulated spine head (Figure 1C).

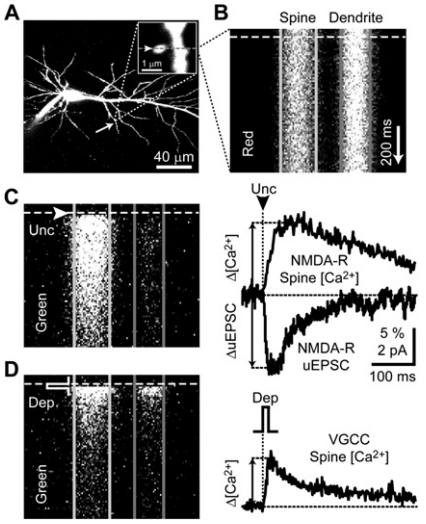

Figure 1. Simultaneous Two-Photon Glutamate Uncaging and Two-Photon [Ca^{2+}] Imaging

(A) CA1 pyramidal neuron. Inset shows a high-magnification image of a dendritic spine. The arrow indicates the location of two-photon glutamate uncaging; the dashed line indicates the position of the line scan.

(B) Red (Ca^{2+}-insensitive) fluorescence is stable during line scan. The dashed line indicates the time of stimulus delivery. Gray lines show demarcations of two regions of interest for analysis of [Ca^{2+}] in spine head (left) and parent dendrite (right).

(C) Green (Ca^{2+}-sensitive) fluorescence change (single trial) in response to two-photon glutamate uncaging (arrow). The right-hand graph shows corresponding NMDA-R [Ca^{2+}] transient in the spine head (top) and the simultaneously recorded average NMDA-R uEPSC (bottom) (average of four trials).

(D) Green fluorescence change for interleaved trials where VGCCs were activated by somatic depolarization.

To control for possible changes in the imaging conditions, or changes in Ca^{2+} handling (e.g., Ca^{2+} buffering and extrusion), we interleaved uncaging stimuli with membrane depolarizations imposed by the somatic patch pipette. Such depolarizations open VGCCs in spines and dendrites and causes global Ca^{2+} influx (Sabatini et al., 2002). The resulting Ca^{2+} accumulations (Figure 1D) were similar to those evoked by back-propagating action potentials (Yasuda et al., 2003).

Plasticity of NMDA-R-Mediated [Ca^{2+}] Signaling

We measured NMDA-R-mediated ΔuEPSC and Δ[Ca^{2+}] before and after delivering four low-frequency uncaging trains (repeated every 10 s; 13 glutamate pulses at 3.3 Hz per train) (Figure 2A). Uncaging trains induced robust (Figures 2B–2E) and long-lasting (>40 min, Figure 2F) ΔuEPSC depression (−30.5% ± 4.5%, p = 0.01), which we call uncaging-evoked long-term depression of NMDA-Rs ($uLTD_{NMDA-R}$).

Surprisingly, depression in Δ[Ca^{2+}] was substantially larger than $uLTD_{NMDA-R}$ (−61.4% ± 6.3% reduction, p = 0.0002); as a result the Ca^{2+} concentration per unit of

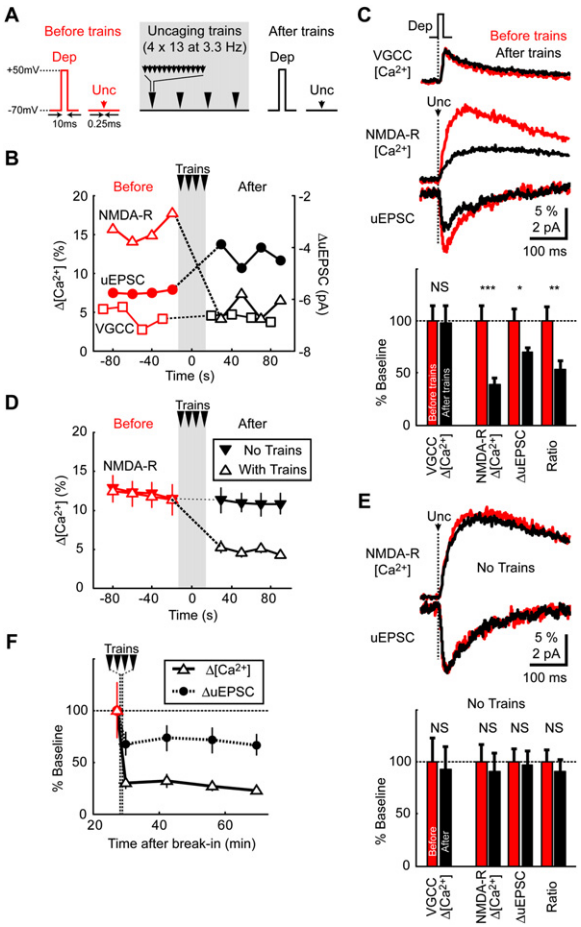

Figure 2. Activity-Dependent Depression of NMDA-Rs in Spines

(A) Schematic diagram of the experimental protocol.

(B) Single spine [Ca^{2+}] amplitudes (NMDA-R, triangles; VGCC, squares) and NMDA-R uEPSC amplitudes (filled circles) in individual trials before (red) and after (black) uncaging trains (A).

(C) The top panel shows spine [Ca^{2+}] transients and uEPSCs averaged across all imaged spines recorded before (red) and after (black) uncaging trains. The bottom panel shows quantification (n = 29 spines; N = ten cells). "Ratio" denotes "$\Delta[Ca^{2+}]/\Delta$uEPSC."

(D) NMDA-R $\Delta[Ca^{2+}]$ for individual trials averaged across all spines for spines stimulated with uncaging trains (open triangles, data as in [B] and [C]) and neighboring spines not stimulated with uncaging trains (filled triangles, n = 23 spines; N = four cells).

(E) Same as (C) for neighboring spines where uncaging trains were omitted from the protocol.

(F) Depression of NMDA-R $\Delta[Ca^{2+}]$ and ΔuEPSC is long lasting (n = nine spines; N = four cells). Error bars, SEM.

NMDA-R, current in spines also decreased ($\Delta[Ca^{2+}]/\Delta$uEPSC; −46.8% ± 8.9%, p = 0.005; Figure 2C). In the absence of uncaging trains, ($\Delta[Ca^{2+}]/\Delta$uEPSC) was stable (−4.7% ± 11.5% change, p = 0.77, Figures 2D and 2E). Under baseline conditions, $\Delta[Ca^{2+}]$ and ΔuEPSC were proportional to each other over a large range of ΔuEPSC (Figure 6G in [Sobczyk et al., 2005]). Therefore, in addition to inducing $uLTD_{NMDA\text{-}R}$, uncaging trains reduced NMDA-R-mediated Ca^{2+} accumulations through another mechanism.

What mechanisms could contribute to the use-dependent decrease in ($\Delta[Ca^{2+}]$ / ΔuEPSC)? In addition to the amount of Ca^{2+} influx, under our experimental conditions spine [Ca^{2+}] is shaped by the following: 1) the strength of Ca^{2+} buffering and extrusion (Ca^{2+} handling), 2) the spine volume, because for fixed Ca^{2+} influx, $\Delta[Ca^{2+}]$ is expected to decrease with increasing spine volume (Nimchinsky et al., 2004; Sobczyk et al., 2005), and 3) spine neck geometry, which determines the diffusional coupling between the spine head and parent dendrite (Noguchi et al., 2005; Sobczyk et al., 2005; Svoboda et al., 1996). We next investigated whether these factors are involved in the activity-dependent reduction of NMDA-R-mediated $\Delta[Ca^{2+}]$.

Imaging conditions and Ca^{2+} handling were unchanged by uncaging trains because VGCC-mediated [Ca^{2+}] transients were stable (−1.6% ± 16.5%, p = 0.93; Figure 2C). Moreover, repetitive uncaging did not alter the time course of [Ca^{2+}] transients (Figure S2). Uncaging trains also did not change spine volumes (−0.5% ± 9.7%, p = 0.97; Figures S3A and S3B and Experimental Procedures). Protocols similar to ours have been shown to induce LTP and enlargement of individual dendritic spines (Matsuzaki et al., 2004) (unpublished data). However, these structural changes were absent when experiments were performed in whole-cell configuration most likely because of washout of LTP (Matsuzaki et al., 2004).

To test for activity-dependent effects on diffusional compartmentalization by spine necks, we performed fluorescence recovery after photobleaching (FRAP) experiments. We measured the FRAP time constant, τ_{FRAP}, before and after induction of depression (see Experimental Procedures). τ_{FRAP}, which is directly related to the geometry of spine necks (Svoboda et al., 1996), was not changed by uncaging trains (−2.5% ± 11.1%, p = 0.95; Figures S3A and S3B). Our experiments therefore argue that depression of ($\Delta[Ca^{2+}]/\Delta$uEPSC) was due to a decrease in the Ca^{2+} influx per unit of NMDA-R current and thus reflects a use-dependent reduction in the fractional Ca^{2+} current through synaptic NMDA-Rs.

Mechanisms Underlying NMDA-R Plasticity

We dissected the mechanisms that trigger depression of the fractional Ca^{2+} current ($\Delta[Ca^{2+}]/\Delta$uEPSC) (Figure 3 and Figure S4). Induction of depression did not require activation of metabotropic glutamate receptors because uncaging trains depressed ΔuEPSC and $\Delta[Ca^{2+}]$ in the presence of a nonselective mGluR antagonist (MCPG, 200 μM). However, blockers of NR2B-containing NMDA-Rs (Ifenprodil, 3 μM; or 0.6 μM Ro25-6981) abolished depression of ($\Delta[Ca^{2+}]/\Delta$uEPSC). Because Ifenprodil and Ro25-6981 reduced the amplitude of the baseline ΔuEPSC (−29.4% ± 7.1%, p = 0.05 for Ifenprodil; Figure S5), it is possible that its effects are not dependent on its subunit specificity but instead are due to reduced overall activation of NMDA-Rs. We therefore blocked baseline ΔuEPSC to similar levels (−36.5% ± 7.2%,

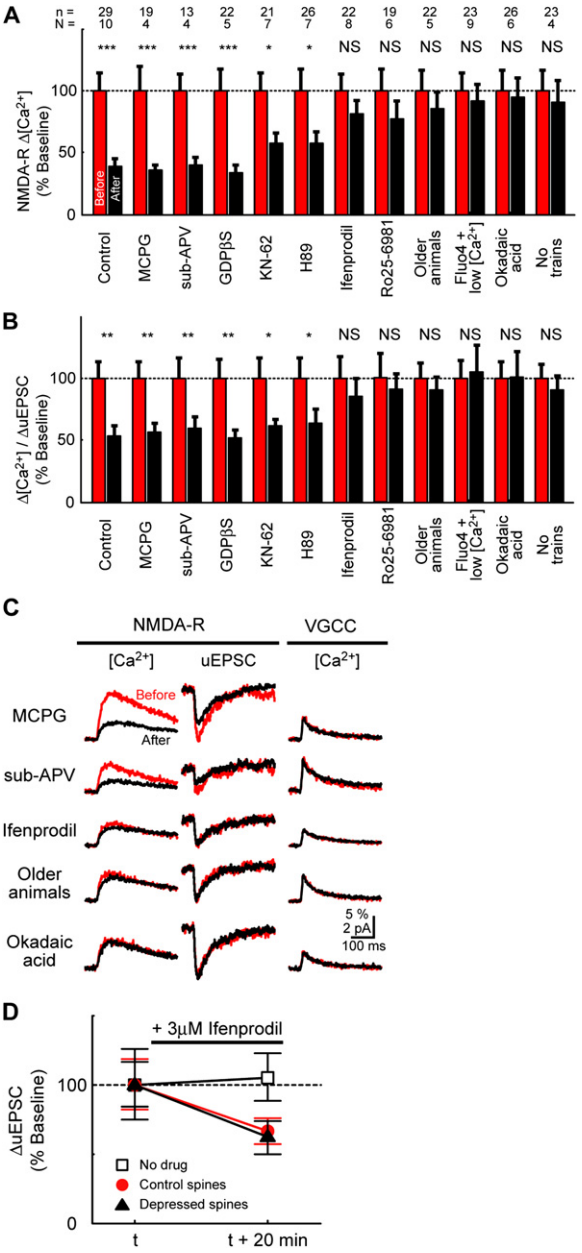

Figure 3. Mechanisms of Induction of NMDA-R Depression

(A) Depression of $\Delta[Ca^{2+}]$ under various conditions (***$p < 0.001$, **$p < 0.01$, *$p < 0.05$; NS, non-significant, $p > 0.4$; red, before trains; black, after trains). "n" indicates the number of recorded spines, and "N" indicates the number of cells.

(B) Same as (A), except for ($\Delta[Ca^{2+}]$/ΔuEPSC) (NS, $p > 0.5$).

(C) Examples of $[Ca^{2+}]$ transients (uncaging, left; depolarizations, right) and uEPSCs (middle) averaged across spines.

(D) Control and depressed spines have identical sensitivity to Ifenprodil. NMDA-R ΔuEPSCs change was measured after wash-in of Ifenprodil (3 μM; applied for ~20 min) for two groups of spines: control (−33.7% ± 9.7%; red circles; n = eight spines; N = five cells) and spines that were previously depressed with uncaging trains (−38.4% ± 11.6%; black triangles; n = eight spines; N = five cells; protocol same as in Figure 2A). ΔuEPSC was constant when Ifenprodil was not added to the bath (5.2% ± 17.5%; open squares; n = 12 spines; N = five cells). Error bars, SEM.

$p = 0.04$; Figure S5) with subsaturating concentrations of a subunit nonspecific antagonist (APV, 1 μM). Under these conditions, depression of ($\Delta[Ca^{2+}]$/ΔuEPSC) still occurred. Therefore depression of ($\Delta[Ca^{2+}]$/ΔuEPSC) required the activation of NR2B-containing NMDA-Rs. During the first month of life, NR1/NR2B receptors are replaced by receptors containing NR2A subunits (Monyer et al., 1994; Quinlan et al., 1999; Sheng et al., 1994). Consistent with these NMDA-R subunit changes at cortical synapses, uncaging trains did not induce depression of ΔuEPSC or $\Delta[Ca^{2+}]$ in older animals (postnatal day 27–28) (Figures 3A–3C).

To determine whether high postsynaptic Ca^{2+} accumulations are critical for the induction of depression, we reduced peak $[Ca^{2+}]$ by loading neurons with 500 μM Fluo4 (an indicator with higher affinity for Ca^{2+} than Fluo4FF [Yasuda et al., 2004]) and lowering extracellular $[Ca^{2+}]$ by a factor of 4 (to 0.5 mM in ACSF). Under these conditions, uncaging-evoked $[Ca^{2+}]$ changes were reduced by a factor of ~10 compared to our standard conditions (see Supplemental Data and Figure 4A). Depression of ($\Delta[Ca^{2+}]$/ΔuEPSC) was blocked, indicating that Ca^{2+}-dependent signaling is required.

Inhibitors of kinases associated with long-term potentiation (CaMKII, KN-62, 10 μM; PKA, H89, 10 μM) did not block depression of ($\Delta[Ca^{2+}]$/ΔuEPSC). However, Okadaic acid (1 μM), a potent inhibitor of serine and threonine phosphatases, completely abolished depression of $\Delta[Ca^{2+}]$ and ΔuEPSC (Figures 3A–3C).

Previous studies have shown that spines with high levels of NR2B-containing NMDA-Rs have the largest NMDA-R-mediated $\Delta[Ca^{2+}]$ (Sobczyk et al., 2005). It is therefore possible that depression of ($\Delta[Ca^{2+}]$/ΔuEPSC) is associated with a substitution of NR2B-containing receptors for NR2A-containing receptors. However, the fact that induction of depression did not change the Ifenprodil sensitivity of NMDA-R-mediated currents argued against this possibility (Figure 3D). Also, blocking dynamin-dependent endocytosis by loading neurons with a nonhydrolyzable GDP analog (600 μM GDPβS) (Morishita et al., 2005) did not alter depression (Figures 3A and 3B), suggesting that receptor trafficking is not involved. Overall, our data indicate that depression of fractional NMDA-R Ca^{2+} currents shares mechanisms of induction with NMDA-R LTD induced with synaptic stimulation (Morishita et al., 2005).

All-or-None Plasticity of NMDA Receptors in Single Spines

Measurements of plasticity at individual synapses, including LTP (Bagal et al., 2005; O'Connor et al., 2005; Petersen et al., 1998), LTD (O'Connor et al., 2005), and depression of VGCCs (Yasuda et al., 2003), have suggested that populations of receptors and channels in individual spines can switch their properties collectively. Two types of experiments revealed that populations of NMDA-Rs in single spines also depress in an all-or-none manner. First, lowering $[Ca^{2+}]$ accumulations in spines by a factor of ~4 (by the

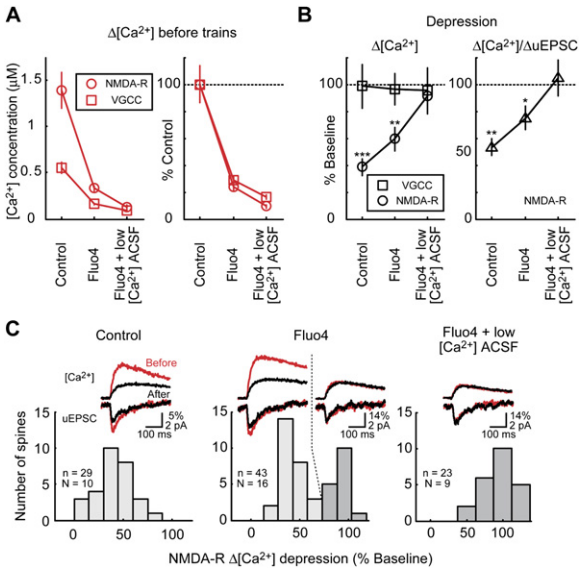

Figure 4. NMDA-R Depression Is Ca^{2+} Dependent

(A) The left graph shows the baseline $\Delta[Ca^{2+}]$ (uncaging, circles; depolarizations, squares) in control conditions (500 μM Fluo4FF) compared to recordings made with Fluo4 (500 μM) in standard ACSF and reduced $[Ca^{2+}]$ ACSF ($[Ca^{2+}]_{ACSF}$ = 0.5 mM). The right graph shows the same data normalized to control.

(B) Magnitude of $\Delta[Ca^{2+}]$ (left) and ($\Delta[Ca^{2+}]/\Delta$uEPSC) (right) depression under different conditions.

(C) Histograms of $\Delta[Ca^{2+}]$ depression for individual spines (data from [A] and [B]). The top graphs show the corresponding average $[Ca^{2+}]$ and uEPSC traces before and after uncaging trains. Under conditions where $\Delta[Ca^{2+}]$ is partially blocked ("Fluo4"), about half of the spines showed $\Delta[Ca^{2+}]$ and ΔuEPSC depression similar to control conditions (light gray), whereas NMDA-Rs in other spines failed to depress (dark gray). Error bars, SEM.

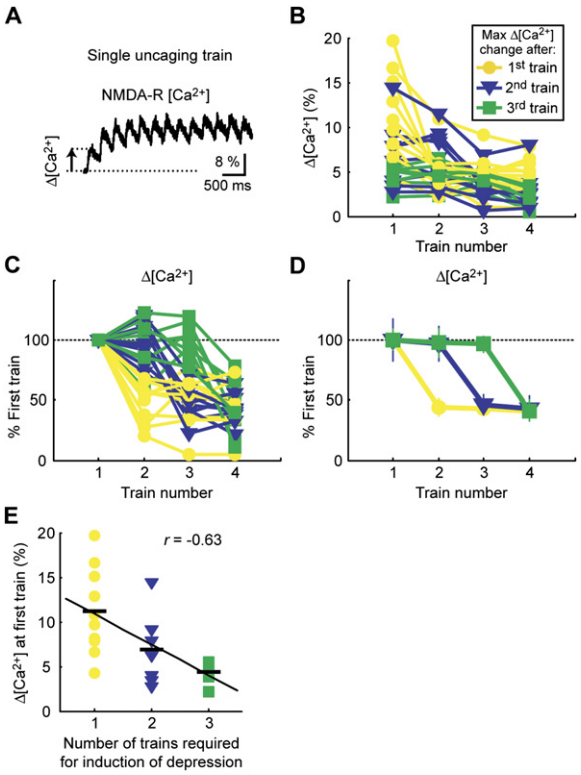

Figure 5. All-or-None NMDA-R Depression

(A) Example of $[Ca^{2+}]$ transient evoked by a single uncaging train.

(B) Amplitudes of $[Ca^{2+}]$ responses to the first stimulus for each of four trains (n = 27 spines; N = 10 cells). Data was color-coded so that the timing of the largest fractional change in $\Delta[Ca^{2+}]$ between trains (defined as $(\Delta[Ca^{2+}]_{j+1} - \Delta[Ca^{2+}]_j)/\Delta[Ca^{2+}]_j$, where j = 1, 2, 3 denotes train number) was indicated.

(C) Same as (B), but normalized to $\Delta[Ca^{2+}]$ of the first train.

(D) Same as (C), but averaged across groups.

(E) Correlation between initial $\Delta[Ca^{2+}]$ and number of trains required for inducing the depression. See also Figure S6. Error bars, SEM.

loading of neurons with Fluo4 at standard extracellular Ca^{2+} concentration, Figure 4A) partially blocked depression of ($\Delta[Ca^{2+}]/\Delta$uEPSC) when the mean of multiple experiments was examined (Figure 4B). However, an analysis of individual spines revealed that under these conditions, some spines showed full $\Delta[Ca^{2+}]$ (~60%) and ΔuEPSC (~30%) depression, whereas other spines did not change (Figure 4C).

Second, we tracked the behavior of NMDA-Rs during the induction protocol. We measured $\Delta[Ca^{2+}]$ produced by the first stimulus in each of the four uncaging trains (Figures 5A and 5B). (In contrast to uEPSC measurements, the Ca^{2+} imaging data had sufficient signal-to-noise ratio for detecting depression in single trials). An unbiased, automated analysis revealed that spine $\Delta[Ca^{2+}]$ depressed to its maximum extent after one of the uncaging trains; further decrease in $\Delta[Ca^{2+}]$ with additional uncaging trains was not observed (Figure 5 and Figure S6). In individual spines, depression occurred after different numbers of trains: In some spines, $\Delta[Ca^{2+}]$ depressed immediately after the first train (by ~60%) (Figures 5C and 5D, yellow), whereas for others, two or three trains were required (Figures 5C and 5D, blue and green). All spines showed $\Delta[Ca^{2+}]$ depression by the fourth train. Spines with bigger initial $\Delta[Ca^{2+}]$ required fewer uncaging trains for depression (correlation coefficient $r = -0.63$, p = 0.0005, Figure 5E), consistent with Ca^{2+}-dependent mechanisms of induction (Figure 4). Our findings indicate that populations of NMDA-Rs in single spines depress collectively, in an all-or-none manner. Furthermore, because depression occurred rapidly (<10 s, the interval between trains), it is likely that the mechanisms of expression involve modification of NMDA-Rs at the synapse rather than receptor trafficking.

DISCUSSION

By combining single-spine glutamate uncaging with measurements of NMDA-R currents and NMDA-R-mediated $[Ca^{2+}]$ changes, we studied the function and plasticity of synaptic NMDA-Rs (Figure 1). Brief low-frequency trains of glutamate produced long-term depression of NMDA-R

currents (Figure 2). $uLTD_{NMDA-R}$ required NMDA-R activation and postsynaptic Ca^{2+}-dependent phosphatase signaling (Figures 3 and 4) and therefore resembles NMDA receptor LTD (Morishita et al., 2005; Selig et al., 1995). In addition to the relatively modest $uLTD_{NMDA-R}$, uncaging trains induced a dramatic reduction in [Ca^{2+}] accumulations per unit of NMDA-R current in dendritic spines (Figures 2 and 3).

What are the expression mechanisms of the depression of NMDA-R-dependent Ca^{2+} accumulations? Under our experimental conditions, uncaging trains did not induce detectable long-lasting changes in spine geometry or Ca^{2+} handling, including Ca^{2+} extrusion and buffering (Figures S2 and S3). This implies that the fractional Ca^{2+} current of the NMDA-R is modulated in a use-dependent manner.

We have previously found that NR2B-containing NMDA-Rs are primarily responsible for the large range of NMDA-R-mediated Ca^{2+} signals observed in individual spines (Sobczyk et al., 2005). Here, we show that activation of NR2B-containing receptors is required for $uLTD_{NMDA-R}$ and depression of the fractional Ca^{2+} current of the NMDA-R. The situation is different for plasticity of AMPA-R EPSCs, where LTP (Barria and Malinow, 2005) but not LTD (Morishita et al., 2006) is preferentially induced by the activation of NR2B-containing receptors.

Depression likely does not involve dynamin-dependent endocytosis (Figures 3A and 3B) ([Morishita et al., 2005], but see also [Montgomery et al., 2005]). A covalent modification of the channel or an associated protein closely coupled to the channel pore (Husi et al., 2000) could explain depression. For example, it has been suggested that the PKA pathway can regulate Ca^{2+} permeability of NMDA receptors (Skeberdis et al., 2006).

Based on the maximum amplitude of the synaptic currents that can be evoked with glutamate uncaging (>10 pA) (Sobczyk et al., 2005) and the current through individual receptors (~1 pA), we can estimate the number of NMDA-Rs at spines as ten or greater (Racca et al., 2000). We found that the receptors in one spine depressed together, or not at all (Figure 5). NMDA-R depression is therefore part of an increasing number of phenomena, including LTP (Bagal et al., 2005; O'Connor et al., 2005; Petersen et al., 1998), LTD (O'Connor et al., 2005), and depression of VGCCs (Yasuda et al., 2003), that exhibit collective behavior of channels and receptors in individual postsynaptic densities. Thus, individual synapses switch between a few, possibly only two, discrete states. Discrete, rather than graded, synapses may be less susceptible to noise and drift (Petersen et al., 1998).

How do our stimuli correspond to plasticity protocols involving synaptic transmission? Uncaging-evoked [Ca^{2+}] accumulations in our experiments are on the same order or lower than those measured during the induction of LTP (Muller and Connor, 1991; Sabatini et al., 2002) (Table S1). The [Ca^{2+}] accumulations achieved in our experiments thus lie within a standard physiological range. Consistently, the protocol we use to induce $uLTD_{NMDA-R}$ also causes LTP of AMPA-R-mediated synaptic transmission (Matsuzaki et al., 2004) (data not shown). (However, note that under our experimental conditions of prolonged whole-cell measurement, LTP was abolished by "washout"; see also Matsuzaki et al. [2004].)

Because of the central role of NMDA-R-mediated Ca^{2+} accumulations in the induction of synaptic plasticity (Bliss and Collingridge, 1993; Malenka and Bear, 2004), activity-dependent depression of NMDA-R-mediated Δ[Ca^{2+}] in spines likely acts as a regulator of synaptic plasticity (Abraham and Bear, 1996). It has previously been shown that relatively weak stimuli can inhibit the induction of LTP with subsequent strong stimuli (Huang et al., 1992). These stimuli likely induced use-dependent reduction of the NMDA-R fractional Ca^{2+} current and caused an increase in the threshold for LTP induction. The activity-dependent tuning of the fractional Ca^{2+} current could thus implement a sliding threshold for synaptic plasticity, which is critical for stabilizing activity levels in neural networks with Hebbian synapses (Bienenstock et al., 1982).

EXPERIMENTAL PROCEDURES

Preparation and Electrophysiology

Acute hippocampal brain slices (300 μm thick) from Sprague-Dawley rats (postnatal day 16–17 unless otherwise stated) were cut as described (Sobczyk et al., 2005) in accordance with animal care and use guidelines of Cold Spring Harbor Laboratory. Slices were incubated in gassed (95% O_2/5% CO_2) artificial CSF (ACSF) containing (in mM) the following: 127 NaCl, 25 $NaHCO_3$, 25 D-glucose, 2.5 KCl, 1.0 $MgCl_2$, 2.0 $CaCl_2$, and 1.25 NaH_2PO_4 at 34°C for 30–45 min and then at room temperature (23°C–25°C) until used. Experiments were performed at room temperature in standard ACSF containing (in mM) the following: 0.1 $MgCl_2$, 2.0 $CaCl_2$, 0.01 NBQX, 0.001 TTX, 0.001 Thapsigargin, 0.02 Ryanodine, 0.01 D-Serine, and 2.5 MNI-caged-L-glutamate. MNI-caged-L-glutamate, NBQX, and Thapsigargin were from Tocris, TTX was from Calbiochem, Ca^{2+} indicators were from Molecular Probes, and all other reagents were from Sigma.

Voltage-clamp whole-cell recordings (V_{hold} = −70 mV) from CA1 pyramidal neurons were made with pipettes (4–6 MΩ) containing the following Cs-based internal solution (in mM): 135 $CsMeSO_3$, 10 HEPES, 10 Na-phosphocreatine, 4 $MgCl_2$, 4 Na_2-ATP, 0.4 Na-GTP, 3 ascorbate, 0.03 Alexa 594 (red, *R*, Ca^{2+}-insensitive), and either 0.5 Fluo4FF or 0.5 Fluo4 (green, *G*, Ca^{2+}-sensitive). We recorded NMDA-R-mediated uncaging-evoked postsynaptic currents (uEPSCs) at the soma. The current amplitude, ΔuEPSC, was computed as the mean amplitude of the uEPSC during a 6 ms window around the peak.

Two-Photon Glutamate Uncaging and [Ca^{2+}] Imaging

We used a custom-built two-photon uncaging and imaging microscope (Sobczyk et al., 2005) powered by two Ti:sapphire pulsed lasers (Mira, Coherent, tuned to 810 nm for Ca^{2+} imaging and MaïTai, Spectra Physics, tuned to 720 nm for glutamate uncaging). The intensity of each laser beam was independently controlled with electro-optical modulators (350–80 LA, Conoptics). Beams were combined with polarized optics and went through the same set of scan mirrors and 60×, 0.9 NA objective (Olympus). Fluorescence was detected by the summation of epifluorescence and transfluorescence signals as described (Mainen et al., 1999a). Image acquisition and glutamate uncaging were controlled by ScanImage (Pologruto et al., 2003).

$[Ca^{2+}]$ imaging was performed in line-scan mode with 2 ms temporal resolution (Sabatini and Svoboda, 2000; Yasuda et al., 2003) by repetitive scanning of line intersecting the dendritic spine and its parent dendrite (Figure 1). In each imaging trial, photomultiplier offsets were measured before shutter opening, followed by the measurement of baseline fluorescence and delivery of stimulus. Fluorescence was monitored for 900 ms after the stimulus.

Each spine was stimulated at 0.05 Hz by depolarizations imposed by the recording pipette at the soma (from −70 mV to +50 mV for 10 ms) and (in interleaved trials) by two-photon glutamate uncaging of MNI-glutamate with brief laser flashes (0.25 ms; wavelength, 720 nm). Individual spines were stimulated four times by somatic depolarizations and four times by glutamate uncaging before and after delivery of uncaging trains (Figure 2B). The standard uncaging location was ~0.5 μm from the center of the spine head in the direction away from the parent dendrite (Figures 1A and 1C). On a 50 μm stretch of dendrite, we selected 1–4 spines that were well separated from their parent dendrite and neighboring spines. The uncaging distance was >1.0 μm from the dendrite. This ensured that uEPSCs reflect the activation of NMDA-Rs on single spines (Sobczyk et al., 2005). $uLTD_{NMDA\text{-}R}$ is unlikely to be caused by phototoxicity because it can be blocked with high concentrations of intracellular Ca^{2+} buffers, phosphatase inhibitors, and other perturbations (Figure 3).

$[Ca^{2+}]$ transients were measured as the ratio of the change in the Ca^{2+}-sensitive green fluorescence over the Ca^{2+}-insensitive red fluorescence in regions of interest (ROI) corresponding to the spine and parent dendrite ($[Ca^{2+}] \equiv 100\ (G/R)/(G/R)_{max,}$ expressed in %, where $(G/R)_{max}$ denotes the maximum fluorescence at saturating Ca^{2+}) (Nimchinsky et al., 2004; Yasuda et al., 2003) (Figures 1B–1D). The mean amplitude of the $[Ca^{2+}]$ transient ($\Delta[Ca^{2+}]$) was computed in a window 40–100 ms after glutamate uncaging (for NMDA-R responses, Figure 1C) or 10–30 ms after the onset of the depolarization pulse (for VGCC responses, Figure 1D). Because the largest fluorescence signals did not exceed 0.2 $(G/R)_{max}$, (G/R) was proportional to $[Ca^{2+}]$ with sublinearity of less than 20% (Yasuda et al., 2004). This sublinearity causes a slight underestimate of the activity-dependent changes in $[Ca^{2+}]$ transient amplitudes.

Estimation of Spine Volume

Spine volume was estimated as described previously (Nimchinsky et al., 2004; Sabatini and Svoboda, 2000; Sobczyk et al., 2005), by computing the ratio of peak spine brightness, which is proportional to the spine volume, over the peak intensity of the big apical dendrite.

Fluorescence Recovery after Photobleaching

In fluorescence recovery after photobleaching (FRAP) experiments, Alexa 594 dye was bleached in spines by ~30% (repeated at least five times) (Figure S3A). Average FRAP traces were fitted with single exponentials for determining the recovery time constant τ_{FRAP} (Figure S3B), which serves as an estimate of the strength of spine-dendrite diffusional coupling (Svoboda et al., 1996).

Data Analysis

Online and offline analysis for electrophysiology and Ca^{2+} imaging were performed with custom-written software in Matlab (Mathworks). Data is given as mean ± SEM. Significance was set at $p = 0.05$ (t test). "n" indicates the number of recorded spines, and "N" indicates the number of cells.

Supplemental Data

Supplemental Data include equations, six figures, and one table and can be found with this article online at http://www.neuron.org/cgi/content/full/53/1/17/DC1/.

ACKNOWLEDGMENTS

We thank T. O'Connor and B. Burbach for technical assistance, R. Malinow, R. Yasuda, V. Scheuss, B. Li, C. Harvey, and D. O'Connor for critical reading of the manuscript, and members of the Svoboda laboratory for comments. This work was supported by the National Institutes of Health and the Howard Hughes Medical Institute.

Received: September 18, 2006
Revised: October 23, 2006
Accepted: November 16, 2006
Published: January 3, 2007

REFERENCES

Abraham, W.C., and Bear, M.F. (1996). Metaplasticity: The plasticity of synaptic plasticity. Trends Neurosci. *19*, 126–130.

Bagal, A.A., Kao, J.P., Tang, C.M., and Thompson, S.M. (2005). Long-term potentiation of exogenous glutamate responses at single dendritic spines. Proc. Natl. Acad. Sci. USA *102*, 14434–14439.

Barria, A., and Malinow, R. (2005). NMDA receptor subunit composition controls synaptic plasticity by regulating binding to CaMKII. Neuron *48*, 289–301.

Bienenstock, E.L., Cooper, L.N., and Munro, P.W. (1982). Theory for the development of neuron selectivity: Orientation specificity and binocular interaction in visual cortex. J. Neurosci. *2*, 32–48.

Bliss, T.V.P., and Collingridge, G.L. (1993). A synaptic model of memory: Long-term potentiation in the hippocampus. Nature *361*, 31–39.

Carter, A.G., and Sabatini, B.L. (2004). State-dependent calcium signaling in dendritic spines of striatal medium spiny neurons. Neuron *44*, 483–493.

Collingridge, G.L., Kehl, S.J., and McLennan, H. (1983). The antagonism of amino acid-induced excitations of rat hippocampal CA1 neurones in vitro. J. Physiol. *334*, 19–31.

Cull-Candy, S., Brickley, S., and Farrant, M. (2001). NMDA receptor subunits: Diversity, development and disease. Curr. Opin. Neurobiol. *11*, 327–335.

Cummings, J.A., Mulkey, R.M., Nicoll, R.A., and Malenka, R.C. (1996). Ca^{2+} signaling requirements for long-term depression in the hippocampus. Neuron *16*, 825–833.

Dudek, S.M., and Bear, M.F. (1992). Homosynaptic long-term depression in area CA1 of hippocampus and effects of N-methyl-D-aspartate receptor blockade. Proc. Natl. Acad. Sci. USA *89*, 4363–4367.

Engert, F., and Bonhoeffer, T. (1999). Dendritic spine changes associated with hippocampal long-term synaptic plasticity. Nature *399*, 66–70.

Furuta, T., Wang, S.S., Dantzker, J.L., Dore, T.M., Bybee, W.J., Callaway, E.M., Denk, W., and Tsien, R.Y. (1999). Brominated 7-hydroxycoumarin-4-ylmethyls: Photolabile protecting groups with biologically useful cross-sections for two photon photolysis. Proc. Natl. Acad. Sci. USA *96*, 1193–1200.

Garaschuk, O., Schneggenburger, R., Schirra, C., Tempia, F., and Konnerth, A. (1996). Fractional Ca2+ currents through somatic and dendritic glutamate receptor channels of rat hippocampal CA1 pyramidal neurones. J. Physiol. *491*, 757–772.

Ghosh, A., Ginty, D.D., Bading, H., and Greenberg, M.E. (1994). Calcium regulation of gene expression in neuronal cells. J. Neurobiol. *25*, 294–303.

Hestrin, S., Nicoll, R.A., Perkel, D.J., and Sah, P. (1990). Analysis of excitatory synaptic action in pyramidal cells using whole- cell recording from rat hippocampal slices. J. Physiol. *422*, 203–225.

Huang, Y.Y., Colino, A., Selig, D.K., and Malenka, R.C. (1992). The influence of prior synaptic activity on the induction of long-term potentiation. Science *255*, 730–733.

Husi, H., Ward, M.A., Choudhary, J.S., Blackstock, W.P., and Grant, S.G. (2000). Proteomic analysis of NMDA receptor-adhesion protein signaling complexes. Nat. Neurosci. *3*, 661–669.

Kauer, J.A., Malenka, R.C., and Nicoll, R.A. (1988). A persistent postsynaptic modification mediates long-term potentiation in the hippocampus. Neuron *1*, 911–917.

Kullmann, D.M. (2003). Silent synapses: What are they telling us about long-term potentiation? Philos. Trans. R. Soc. Lond. B Biol. Sci. *358*, 727–733.

Kutsuwada, T., Kashiwabuchi, N., Mori, H., Sakimura, K., Kushiya, E., Araki, K., Meguro, H., Masaki, H., Kumanishi, T., Arakawa, M., et al. (1992). Molecular diversity of the NMDA receptor channel. Nature *358*, 36–41.

Mainen, Z.F., Maletic-Savatic, M., Shi, S.H., Hayashi, Y., Malinow, R., and Svoboda, K. (1999a). Two-photon imaging in living brain slices. Methods *18*, 231–239.

Mainen, Z.F., Malinow, R., and Svoboda, K. (1999b). Synaptic calcium transients in single spines indicate that NMDA receptors are not saturated. Nature *399*, 151–155.

Malenka, R.C., and Bear, M.F. (2004). LTP and LTD: An embarrassment of riches. Neuron *44*, 5–21.

Maletic-Savatic, M., Malinow, R., and Svoboda, K. (1999). Rapid dendritic morphogenesis in CA1 hippocampal dendrites induced by synaptic activity. Science *283*, 1923–1927.

Matsuzaki, M., Ellis-Davies, G.C., Nemoto, T., Miyashita, Y., Iino, M., and Kasai, H. (2001). Dendritic spine geometry is critical for AMPA receptor expression in hippocampal CA1 pyramidal neurons. Nat. Neurosci. *4*, 1086–1092.

Matsuzaki, M., Honkura, N., Ellis-Davies, G.C., and Kasai, H. (2004). Structural basis of long-term potentiation in single dendritic spines. Nature *429*, 761–766.

Montgomery, J.M., Selcher, J.C., Hanson, J.E., and Madison, D.V. (2005). Dynamin-dependent NMDAR endocytosis during LTD and its dependence on synaptic state. BMC Neurosci. *6*, 48.

Monyer, H., Burnashev, N., Laurie, D.J., Sakmann, B., and Seeburg, P.H. (1994). Developmental and regional expression in the rat brain and functional properties of four NMDA receptors. Neuron *12*, 529–540.

Morishita, W., Lu, W., Smith, G.B., Nicoll, R.A., Bear, M.F., and Malenka, R.C. (2006). Activation of NR2B-containing NMDA receptors is not required for NMDA receptor-dependent long-term depression. Neuropharmacology, in press.

Morishita, W., Marie, H., and Malenka, R.C. (2005). Distinct triggering and expression mechanisms underlie LTD of AMPA and NMDA synaptic responses. Nat. Neurosci. *8*, 1043–1050.

Muller, W., and Connor, J.A. (1991). Dendritic spines as individual neuronal compartments for synaptic Ca^{2+} responses. Nature *354*, 73–76.

Nimchinsky, E.A., Yasuda, R., Oertner, T.G., and Svoboda, K. (2004). The number of glutamate receptors opened by synaptic stimulation in single hippocampal spines. J. Neurosci. *24*, 2054–2064.

Noguchi, J., Matsuzaki, M., Ellis-Davies, G.C., and Kasai, H. (2005). Spine-neck geometry determines NMDA receptor-dependent Ca2+ signaling in dendrites. Neuron *46*, 609–622.

Nusser, Z., Lujan, R., Laube, G., Roberts, J.D., Molnar, E., and Somogyi, P. (1998). Cell type and pathway dependence of synaptic AMPA receptor number and variability in the hippocampus. Neuron *21*, 545–559.

O'Connor, D.H., Wittenberg, G.M., and Wang, S.S. (2005). Graded bidirectional synaptic plasticity is composed of switch-like unitary events. Proc. Natl. Acad. Sci. USA *102*, 9679–9684.

Petersen, C.C., Malenka, R.C., Nicoll, R.A., and Hopfield, J.J. (1998). All-or-none potentiation at CA3–CA1 synapses. Proc. Natl. Acad. Sci. USA *95*, 4732–4737.

Pologruto, T.A., Sabatini, B.L., and Svoboda, K. (2003). ScanImage: Flexible software for operating laser-scanning microscopes. Biomed. Eng. Online *2*, 13.

Quinlan, E.M., Olstein, D.H., and Bear, M.F. (1999). Bidirectional, experience-dependent regulation of N-methyl-D-aspartate receptor subunit composition in the rat visual cortex during postnatal development. Proc. Natl. Acad. Sci. USA *96*, 12876–12880.

Racca, C., Stephenson, F.A., Streit, P., Roberts, J.D., and Somogyi, P. (2000). NMDA receptor content of synapses in stratum radiatum of the hippocampal CA1 area. J. Neurosci. *20*, 2512–2522.

Sabatini, B.L., and Svoboda, K. (2000). Analysis of calcium channels in single spines using optical fluctuation analysis. Nature *408*, 589–593.

Sabatini, B.S., Oertner, T.G., and Svoboda, K. (2002). The life-cycle of Ca^{2+} ions in spines. Neuron *33*, 439–452.

Schneggenburger, R., Zhou, Z., Konnerth, A., and Neher, E. (1993). Fractional contribution of calcium to the cation current through glutamate receptor channels. Neuron *11*, 133–143.

Selig, D.K., Hjelmstad, G.O., Herron, C., Nicoll, R.A., and Malenka, R.C. (1995). Independent mechanisms for long-term depression of AMPA and NMDA responses. Neuron *15*, 417–426.

Sheng, M., Cummings, J., Roldan, L.A., Jan, Y.N., and Jan, L.Y. (1994). Changing subunit composition of heteromeric NMDA receptors during development of rat cortex. Nature *368*, 144–147.

Skeberdis, V.A., Chevaleyre, V., Lau, C.G., Goldberg, J.H., Pettit, D.L., Suadicani, S.O., Lin, Y., Bennett, M.V., Yuste, R., Castillo, P.E., and Zukin, R.S. (2006). Protein kinase A regulates calcium permeability of NMDA receptors. Nat. Neurosci. *9*, 501–510.

Sobczyk, A., Scheuss, V., and Svoboda, K. (2005). NMDA receptor subunit-dependent [Ca2+] signaling in individual hippocampal dendritic spines. J. Neurosci. *25*, 6037–6046.

Svoboda, K., Tank, D.W., and Denk, W. (1996). Direct measurement of coupling between dendritic spines and shafts. Science *272*, 716–719.

Takumi, Y., Ramirez-Leon, V., Laake, P., Rinvik, E., and Ottersen, O.P. (1999). Different modes of expression of AMPA and NMDA receptors in hippocampal synapses. Nat. Neurosci. *2*, 618–624.

Vanhoutte, P., and Bading, H. (2003). Opposing roles of synaptic and extrasynaptic NMDA receptors in neuronal calcium signalling and BDNF gene regulation. Curr. Opin. Neurobiol. *13*, 366–371.

Wang, X.J. (2002). Probabilistic decision making by slow reverberation in cortical circuits. Neuron *36*, 955–968.

Yasuda, R., Nimchinsky, E.A., Scheuss, V., Pologruto, T.A., Oertner, T.G., Sabatini, B.L., and Svoboda, K. (2004). Imaging calcium concentration dynamics in small neuronal compartments. Sci. STKE *2004*, pl5.

Yasuda, R., Sabatini, B.L., and Svoboda, K. (2003). Plasticity of calcium channels in dendritic spines. Nat. Neurosci. *6*, 948–955.

Yuste, R., and Bonhoeffer, T. (2001). Morphological changes in dendritic spines associated with long-term synaptic plasticity. Annu. Rev. Neurosci. *24*, 1071–1089.

Yuste, R., and Denk, W. (1995). Dendritic spines as basic functional units of neuronal integration. Nature *375*, 682–684.

Zucker, R.S. (1999). Calcium- and activity-dependent synaptic plasticity. Curr. Opin. Neurobiol. *9*, 305–313.